



Retrieving the paleoclimatic signal from the deeper part of the EPICA Dome C ice core

J.-L. Tison¹, M. de Angelis², G. Littot³, E. Wolff³, H. Fischer⁴, M. Hansson⁵, M. Bigler⁴, R. Udisti⁶, A. Wegner⁷, J. Jouzel⁸, B. Stenni⁹, S. Johnsen^{†,10}, V. Masson-Delmotte⁸, A. Landais⁸, V. Lipenkov¹¹, L. Loulergue², J.-M. Barnola^{†,2}, J.-R. Petit², B. Delmonte¹², G. Dreyfus¹³, D. Dahl-Jensen¹⁰, G. Durand², B. Bereiter⁴, A. Schilt⁴, R. Spahni⁴, K. Pol³, R. Lorrain¹, R. Souchez¹, and D. Samyn¹⁴

¹Laboratoire de Glaciologie, Université Libre de Bruxelles, CP 160/03, 50, av. F.D. Roosevelt, 1050-Bruxelles, Belgium

²Laboratoire de Glaciologie et Géophysique de l'Environnement, 54, Rue Molière Domaine Universitaire
38402 Saint-Martin d'Hères, France

³British Antarctic Survey, High Cross, Madingley Road, Cambridge CB3 0ET, UK

⁴Climate and Environmental Physics, Physics Institute & Oeschger Centre for Climate Change Research, University of Bern,
Sidlerstrasse 5, 3012 Bern, Switzerland

⁵Department of Physical Geography and Quaternary Geology, Stockholm University, 106 91 Stockholm, Sweden

⁶University of Florence. Chemistry Dept., via della Lastruccia, 3 – 50019 Sesto Fiorentino, Florence, Italy

⁷Alfred Wegener Institute, Bremerhaven, Germany

⁸Laboratoire des Sciences du Climat et de l'Environnement/Institut Pierre Simon Laplace, CEA-CNRS-UVSQ, CEA Saclay,
91191, Gif-sur-Yvette, France

⁹Dipartimento di Scienze Ambientali, Informatica e Statistica, Università Ca Foscari, Venezia, Italy

¹⁰Niels Bohr Institute, Juliane Maries Vej 30, 2100 Copenhagen, Denmark

¹¹Arctic and Antarctic Research Institute, 38 Bering Str., St. Petersburg, Russia

¹²DISAT, Dept. of Earth and Environmental Sciences, University Milano Bicocca, Piazza della Scienza 1, 20126 Milano, Italy

¹³Office of Policy and International Affairs, US Department of Energy, Washington, DC 20585, USA

¹⁴Nagaoka University of Technology, 1603-1 Kamitomioka, Nagaoka, Niigata 940-2188, Japan

[†]deceased

Correspondence to: J.-L. Tison (jtison@ulb.ac.be)

Received: 13 January 2015 – Published in The Cryosphere Discuss.: 28 January 2015

Revised: 1 July 2015 – Accepted: 13 July 2015 – Published: 20 August 2015

Abstract. An important share of paleoclimatic information is buried within the lowermost layers of deep ice cores. Because improving our records further back in time is one of the main challenges in the near future, it is essential to judge how deep these records remain unaltered, since the proximity of the bedrock is likely to interfere both with the recorded temporal sequence and the ice properties. In this paper, we present a multiparametric study (δD - $\delta^{18}O_{ice}$, $\delta^{18}O_{atm}$, total air content, CO_2 , CH_4 , N_2O , dust, high-resolution chemistry, ice texture) of the bottom 60 m of the EPICA (European Project for Ice Coring in Antarctica) Dome C ice core from central Antarctica. These bottom layers were subdivided into two distinct facies: the lower 12 m showing vis-

ible solid inclusions (basal dispersed ice facies) and the upper 48 m, which we will refer to as the “basal clean ice facies”. Some of the data are consistent with a pristine paleoclimatic signal, others show clear anomalies. It is demonstrated that neither large-scale bottom refreezing of subglacial water, nor mixing (be it internal or with a local basal end term from a previous/initial ice sheet configuration) can explain the observed bottom-ice properties. We focus on the high-resolution chemical profiles and on the available remote sensing data on the subglacial topography of the site to propose a mechanism by which relative stretching of the bottom-ice sheet layers is made possible, due to the progressively confining effect of subglacial valley sides. This stress

field change, combined with bottom-ice temperature close to the pressure melting point, induces accelerated migration recrystallization, which results in spatial chemical sorting of the impurities, depending on their state (dissolved vs. solid) and if they are involved or not in salt formation. This chemical sorting effect is responsible for the progressive build-up of the visible solid aggregates that therefore mainly originate “from within”, and not from incorporation processes of debris from the ice sheet’s substrate. We further discuss how the proposed mechanism is compatible with the other ice properties described. We conclude that the paleoclimatic signal is only marginally affected in terms of global ice properties at the bottom of EPICA Dome C, but that the timescale was considerably distorted by mechanical stretching of MIS20 due to the increasing influence of the subglacial topography, a process that might have started well above the bottom ice. A clear paleoclimatic signal can therefore not be inferred from the deeper part of the EPICA Dome C ice core. Our work suggests that the existence of a flat monotonic ice–bedrock interface, extending for several times the ice thickness, would be a crucial factor in choosing a future “oldest ice” drilling location in Antarctica.

1 Paleoclimatic signals in basal layers of deep ice cores

Deep ice cores retrieved from the two present-day major ice sheets on Earth, Greenland in the north and Antarctica in the south, delivered a wealth of unique paleoclimatic archives over the last decades. These allowed reconstruction of global climatic and environmental conditions over the last 800 000 years, including unprecedented records of cyclic changes in the composition of greenhouse gases (CO₂, CH₄, N₂O). An important share of that paleoclimatic information is buried within the lowermost sections of those deep ice cores, due to the mechanical thinning of annual accumulation layers with depth. Improving the records further back in time is therefore one of the main challenges of ice core science in the near future (IPICS, 2009). A major concern in this regard is to judge how far down we can trust the paleoclimatic signals stored within the ice, since the proximity of the bedrock is likely to interfere both with the recorded temporal sequence and with the ice properties. This in turn is closely linked to the thermal and hydrological regime at the bottom of the ice sheet, as shown previously in the literature describing basal layers of deep ice cores (e.g. Goodwin, 1993; Gow et al., 1979; Gow and Meese, 1996; Herron and Langway, 1979; Jouzel et al., 1999; Koerner and Fisher, 1979; Souchez, 1997; Souchez et al., 1993, 1995a, b, 2000a, 2002b, 2003, 2006, 1994, 1998; Tison et al., 1994, 1998, Weis et al., 1997). In some cases, where the ice–bedrock interface is clearly below the pressure-melting point (pmp) as, for example, at the GRIP (−9 °C) or the Dye-3 (−12 °C) ice coring sites in Greenland, single or multiple mixing events between

the present-day ice sheet ice and local ice remnants of previous (or even initial) ice sheet configurations are encountered (Souchez, 1997; Souchez et al., 1994, 1998, 2000b; Verbeke et al., 2002). Where the ice–bedrock interface is at the pmp, the meteoric ice has the potential to melt at a rate that would depend on the heat budget at the ice–bedrock interface (geothermal heat flux, internal friction and conduction through the overlying ice). In some cases, where the subglacial topography allows it, like at the Antarctic Vostok site, a subglacial lake will exist. Again, depending on the heat budget but also on the subglacial lake water circulation pattern, lake ice will form at the ice–water interface in substantial amounts (e.g. Jouzel et al., 1999; Souchez et al., 2000a 2002a, 2003). This ice, evidently, does not carry paleoclimatic information. Furthermore, in the case of large subglacial lakes (such as Lake Vostok) where the ice column above can be considered in full hydrostatic equilibrium buoyancy, re-grounding of the ice sheet on the lee side of the lake will induce dynamical perturbations (such as folds), even in the meteoric ice above, as demonstrated for MIS11 (Raynaud et al., 2005) and for the ice just above the accreted lake ice (Souchez et al., 2002a, b, 2003). A less well-documented case, however, is the one where no significant water body exists at the ice–bedrock interface. If only melting occurs at the interface, with no water accumulation and no refreezing (as, for example at the NGRIP site in Greenland), can we then rely on the paleoclimatic information gathered in the basal layers? The EPICA (European Project for Ice Coring in Antarctica) Dome C ice core potentially provides us with an opportunity to investigate that specific case. In this paper, we are using a multiparametric approach, combining new and existing low-resolution (50 cm) data for the bottom 60 m of ice from the EDC (EPICA dome C) ice core with a new high-resolution (1.5 to 8 cm) chemical data set in order to better understand the processes at work and evaluate how these might have altered the environmental archive.

2 The EPICA Dome C ice core

The Dome C deep ice core (EDC) is one of the two ice cores drilled in the framework of the European Project for Ice Coring in Antarctica (EPICA). It is located at Concordia Station (Dome C – 75°06′04″ S; 123°20′52″ E), about 1200 km south of the French coastal station, Dumont d’Urville, and 720 km north-east of the Russian Vostok Station. Detailed GPS surface topography and airborne radar surveys were conducted in 1994–1995 in order to optimize the choice for the drilling location (Remy and Tabacco, 2000; Tabacco et al., 1998). These provided clear features of the bedrock and surface topography, showing a set of north–south-trending parallel valleys around 20 km wide and 200–400 m deep in the bedrock, corresponding to smooth elongated undulations a few metres high at the surface.

A final drilling depth of 3259.72 m was reached in December 2004, about 15 m above the ice–bedrock interface (to prevent from eventually making contact with subglacial meltwaters). The ice temperature was -3°C at 3235 m and a simple extrapolation to the bottom indicates that the melting point should be reached at the interface (Lefebvre et al., 2008). The top ca. 3200 m of the EDC ice core have already been extensively studied and provided a full suite of climatic and environmental data over the last 8 climatic cycles (e.g. Delmonte et al., 2008; Durand et al., 2008; EPICA Community members, 2004; Jouzel et al., 2007; Lambert et al., 2008; Louergue et al., 2008; Lüthi et al., 2008; Wolff et al., 2006). Raisbeck et al. (2006) confirmed the old age of the deep EDC ice by presenting evidence for enhanced ^{10}Be deposition in the ice at 3160–3170 m (corresponding to the 775–786 kyr interval in the EDC2 timescale) consistent with the age and duration of the Matuyama–Brunhes geomagnetic reversal. A coherent interpretation of CO_2 and CH_4 profiles (Lüthi et al., 2008; Louergue et al., 2008) also established the presence of Marine Ice Stages (MIS) 18 (ca. 739–767 kyr BP) and 19 (ca. 767–790 kyr BP). However, a detailed study of the isotopic composition of O_2 and its relationship to daily Northern Hemisphere summer insolation and comparison to marine sediment records showed potentially anomalous flow in the lowermost 500 m of the core with associated distortion of the EDC2 timescale by a factor of up to 2. This led to the construction of the new, currently used, EDC3 timescale (Parrenin et al., 2007). Note that efforts are still ongoing to refine this timescale, combining multi-site data sets and using $\delta^{18}\text{O}_{\text{atm}}$ and O_2/N_2 as proxies for orbital tuning (Landais et al., 2012; Bazin et al., 2013).

As described below, the bottom 60 m of the available core acquired distinctive properties, as a result of processes driven by the proximity of the ice–bedrock interface. We will therefore, in accordance with the previous literature (e.g. Knight, 1997; Hubbard et al., 2009) refer to it as “basal ice”. The last 12 m of the available core show visible solid inclusions (Fig. 1a), which are traditionally interpreted as a sign of interactions with the bedrock. These inclusions are spherical in shape, brownish to reddish in colour, and generally increase both in size and density with increasing depth. They however remain evenly distributed within the ice, therefore qualifying as a “basal dispersed facies” in existing classifications (e.g. Hubbard et al., 2009). Between 3248.30 m (first occurrence of inclusion visible by eye) and 3252.15 m the inclusions are only sparse (0 to 10 inclusions per 55 cm ice core length) and less than 1 mm in diameter. In the lower 8 m, inclusions get bigger (up to 3 mm in the last 50 cm sample) and reach more than 20 individual inclusions per 50 cm ice core length. In several cases, especially for the bigger inclusions, these are “enclosed” in a whitish ovoid bubble-like feature (e.g. upper left corner of Fig. 1a). Careful visual examination of the texture of each individual inclusion suggests that these generally consist of a large number of smaller aggregates although individual particles also occur. In most cases, these

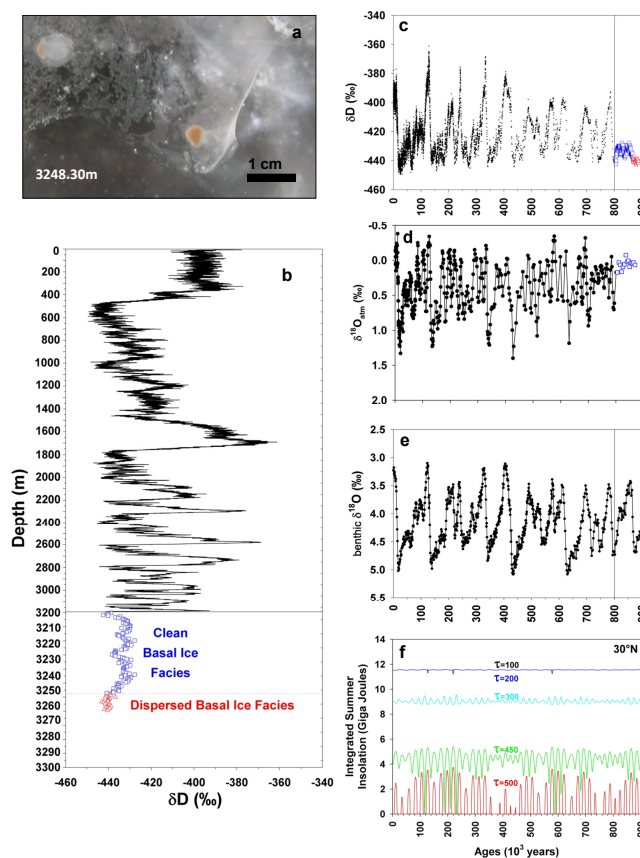


Figure 1. (a) visual appearance of the EDC basal ice in the lower metres of the core (photo: D. Dahl-Jensen), (b) EDC $\delta\text{D}_{\text{ice}}$ vs. depth, (c) EDC $\delta\text{D}_{\text{ice}}$ vs. age (EDC3 timescale extended to the basal ice layers), (d) combined Vostok and EDC $\delta^{18}\text{O}_{\text{atm}}$ vs. age (adapted from Dreyfus et al., 2007), (e) $\delta^{18}\text{O}$ vs. age for the benthic record stack of Lisiecki and Raymo (2005), and (f) integrated summer insolation for various thresholds (τ) at 30°N vs. age, as calculated by Huybers (2006). For reasons described in the text, ice below 3189.45 m depth is referred to as “clean ice facies” (blue squares) and “dispersed ice facies” (red triangles) describes the ice below 3248.30 m, where solid inclusions are visible.

inclusions appear to be located at crystal boundaries. A detailed study of the morphology, mineralogy and chemistry of some of these individual inclusions is described elsewhere (de Angelis et al., 2013). Finally, it should be kept in mind that these characteristics are valid for ice collected between 6 and 15 m above the actual ice–bedrock interface. We do not, unfortunately, have any information on the properties of the ice below, the thickness of which was estimated using a downhole seismometer (J. Schwander, personal communication, 2011). The upper 48 m of the basal ice sequence will be referred to as the “basal clean ice facies” (i.e. devoid of visible inclusions), also in line with previous work (Hubbard et al., 2009).

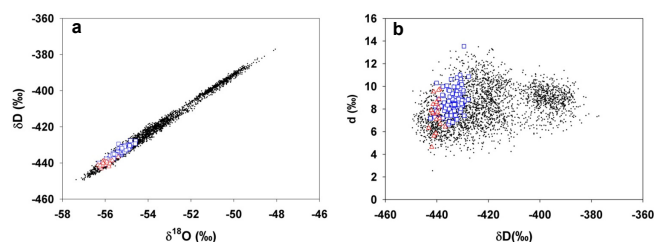


Figure 2. (a) δD_{ice} (‰) vs. $\delta^{18}O_{ice}$ (‰) and (b) d (deuterium excess ‰) vs. δD_{ice} (‰) for the clean (open blue squares) and dispersed (open red triangles) basal ice facies at EPICA Dome C, as compared to the ice from the 0–140 ky interval (black dots, Stenni et al., 2010). See text for details.

3 Material and methods

The dispersed facies of the basal ice of the EDC core shows a relatively low debris content, compared to the other deep ice coring sites described in previous studies (Camp Century, GRIP, Dye-3, Vostok), and could therefore be processed in continuity with the cutting scheme used for the EDC ice above. The multi-parametric data set discussed in this paper was therefore obtained applying analytical techniques described in full in previous studies focusing on single parameters. We are summarizing those in the Supplement, referring to the appropriate previous literature for full details.

4 The basal ice properties: a multiparametric approach

Figure 1b and c plot the full δD profile of the EPICA ice core, vs. depth and age respectively (EDC3 timescale, Parrenin et al., 2007). As stated above, we will use the “dispersed ice facies” terminology for the lower 12 m (red open triangles) and qualify the 48 m above as the “clean ice facies” (blue open squares); “basal ice” will refer to the whole 60 m sequence. A combined Vostok-EDC $\delta^{18}O_{atm}$ profile (isotopic composition of atmospheric oxygen in ice) vs. EDC3 timescale is shown in Fig. 1d (adapted from Dreyfus et al., 2007; Petit et al., 1999 for the ice above 3200 m). The $\delta^{18}O$ benthic record stack of Lisiecki and Raymo (2005) is also plotted as a reference in Fig. 1e. The co-isotopic properties of the EPICA Dome C bottom ice (open squares for clean ice facies, open triangles for dispersed ice facies) are described in Fig. 2a (δD vs. $\delta^{18}O$) and b (d_{excess} vs. δD) and compared to those of the ice from the last 140 ky (Stenni et al., 2010). Work in progress on the co-isotopic properties of the older ice (down to 3189.45 m) shows that the latter do not differ from the trends seen in Fig. 2 (B. Stenni et al., unpublished data).

Figure 3 and Table S1 in Supplement summarize the available low-resolution gas and insoluble dust concentrations data. CH_4 , CO_2 and N_2O are covered for both the clean (squares in Fig. 3a) and dispersed (triangles in Fig. 3a) facies while total gas content (grey dots in Fig. 3a) is only avail-

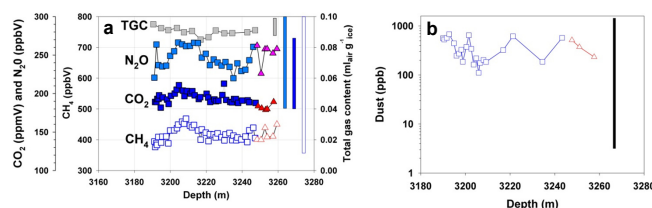


Figure 3. Gas and dust properties of the clean (squares) and dispersed (triangles) basal ice facies at EPICA Dome C: (a) total gas content ($mL_{air} g_{ice}^{-1}$, grey), methane (ppbV, white), nitrous oxide (ppbV, light blue) and carbon dioxide (ppbV, dark blue) – vertical bars of equivalent shading cover the full concentration range observed for CH_4 , CO_2 , N_2O and total gas content during the preceding climatic cycles, (b) dust concentrations (ppb) – the black vertical bar covers the full concentration range during the previous climatic cycles.

able for the clean ice facies. The full concentration ranges observed for CH_4 (Loulergue et al., 2008), CO_2 (Lüthi et al., 2008), N_2O (Schilt et al. 2010) and total gas content (Raynaud et al., 2007) during the preceding climatic cycles are also shown for reference, as white, dark blue, light blue and grey vertical bars respectively. The limited number of dust concentration measurements available is shown in Fig. 3b (same symbols as above) and also compared to the full range of values observed during the previous climatic cycles (black vertical bar, Delmonte et al., 2008).

Clean and dispersed basal ice facies concentrations of selected chemical species (MSA , SO_4 , Ca , Mg , Na , K , Cl , NO_3) are presented in two complementary ways, in Figs. 4 and 5. In Fig. 4 high-resolution (1.5–5 cm) profiles of discrete sections in the clean (open blue squares) and dispersed (open red triangles) facies are shown, along with the 5–8 cm resolution profile in the ice above 3200 m (black dots, courtesy of the EPICA Chemistry Consortium). In Fig. 5, the same data set is re-arranged as a simple frequency distribution within bins of 5 or $1 ng g^{-1}$ depending on the species. Clean facies are plotted as open blue squares on the thick solid blue line and dispersed facies as open red triangles on the thick dotted red line. All data from preceding “full glacial” intervals (i.e. excluding interglacials and complete transitions) are plotted as a background in thin grey lines with incremented symbols (see caption in upper left graph for MSA). Table 1 summarizes the data set used in Fig. 5 in terms of concentration means and 1σ values, with the depth and isotopic ranges associated to each time interval chosen. The “full glacial” intervals were selected on careful analysis of the δD data set, keeping for each glacial period the samples with the lowest values and using the location of increasing isotopic gradient with depth as a cutting point on both sides. We discuss in the supplementary material section why we believe we can compare the results from these various groups of samples shown in Fig. 5 and Table 1, despite the fact that they cover different time windows.

Table 1. Mean concentration and 1σ values (ngg^{-1} or ppb) for selected chemical species in the clean and dispersed basal ice facies of the EPICA Dome C ice core, as compared to those of the previous full glacial periods (see text for details). Depth (m) and δD (‰) ranges are given for each time interval considered.

| Glacial | Depth range (m) | | Isotopic range (δD ‰) | | MSA (ngg^{-1}) | | SO ₄ (ngg^{-1}) | | Ca (ngg^{-1}) | | Mg (ngg^{-1}) | |
|------------------|-----------------|--------|--------------------------------------|--------|---------------------------|----------|---------------------------------------|----------|--------------------------|----------|--------------------------|----------|
| | | | min | max | mean | σ | mean | σ | mean | σ | mean | σ |
| MIS 2 | 507.7 | 583.5 | −449.3 | −432.8 | 18.24 | 7.00 | 213.78 | 85.15 | 43.27 | 14.89 | 19.31 | 4.08 |
| MIS 4 | 1007.6 | 1042.2 | −446.4 | −430.5 | 20.94 | 4.00 | 194.80 | 52.52 | 30.85 | 10.96 | 14.28 | 3.84 |
| MIS 6 | 1801.8 | 1997.0 | −447.1 | −419.8 | 18.60 | 5.00 | 170.01 | 51.73 | 23.60 | 12.25 | 13.54 | 4.04 |
| MIS 8 | 2320.0 | 2398.6 | −444.5 | −421.5 | 27.90 | 6.13 | 192.05 | 50.92 | 23.37 | 12.98 | 14.92 | 4.28 |
| MIS 10 | 2599.9 | 2650.0 | −445.0 | −425.1 | 26.77 | 7.88 | 183.55 | 43.56 | 22.92 | 9.84 | 14.92 | 3.86 |
| MIS 12 | 2783.2 | 2794.9 | −440.9 | −422.5 | 23.44 | 5.04 | 187.36 | 45.54 | 43.47 | 19.09 | 19.82 | 5.50 |
| MIS 14.2 | 2915.7 | 2919.9 | −436.4 | −429.3 | 23.75 | 6.37 | 162.06 | 21.72 | 20.46 | 6.19 | 15.80 | 2.75 |
| MIS 16 | 3037.6 | 3039.8 | −441.0 | −412.3 | 32.61 | 6.95 | 167.86 | 39.55 | 36.09 | 17.21 | 16.37 | 5.84 |
| MIS 18 | 3137.8 | 3153.1 | −441.4 | −423.7 | 36.40 | 23.47 | 195.35 | 139.18 | 31.26 | 19.76 | 20.03 | 25.47 |
| Clean Facies | 3201.0 | 3248.0 | −442.5 | −427.7 | 21.50 | 20.32 | 150.39 | 107.98 | 29.53 | 16.87 | 11.49 | 12.48 |
| Dispersed Facies | 3248.0 | 3259.3 | −443.2 | −436.7 | 25.27 | 18.43 | 139.58 | 91.46 | 42.10 | 29.44 | 16.25 | 11.23 |

| Glacial | Depth range (m) | | Isotopic range (δD ‰) | | Na (ngg^{-1}) | | Cl (ngg^{-1}) | | NO ₃ (ngg^{-1}) | | K (ngg^{-1}) | |
|------------------|-----------------|--------|--------------------------------------|--------|--------------------------|----------|--------------------------|----------|---------------------------------------|----------|-------------------------|----------|
| | | | min | max | mean | σ | mean | σ | mean | σ | mean | σ |
| MIS 2 | 507.7 | 583.5 | −449.3 | −432.8 | 97.37 | 17.54 | 160.68 | 48.64 | 40.93 | 16.01 | 7.45 | 1.89 |
| MIS 4 | 1007.6 | 1042.2 | −446.4 | −430.5 | 79.81 | 17.75 | 129.89 | 25.25 | 29.38 | 12.41 | 4.91 | 2.34 |
| MIS 6 | 1801.8 | 1997.0 | −447.1 | −419.8 | 71.57 | 16.65 | 107.56 | 40.45 | 24.72 | 12.63 | 3.74 | 2.36 |
| MIS 8 | 2320.0 | 2398.6 | −444.5 | −421.5 | 76.76 | 35.00 | 112.06 | 38.05 | 26.24 | 17.20 | 3.84 | 5.24 |
| MIS 10 | 2599.9 | 2650.0 | −445.0 | −425.1 | 77.80 | 32.30 | 112.76 | 61.56 | 30.21 | 19.92 | 5.77 | 9.76 |
| MIS 12 | 2783.2 | 2794.9 | −440.9 | −422.5 | 72.70 | 19.82 | 138.46 | 34.04 | 48.69 | 22.43 | 3.93 | 3.32 |
| MIS 14.2 | 2915.7 | 2919.9 | −436.4 | −429.3 | 70.88 | 15.13 | 110.46 | 21.66 | 34.33 | 17.31 | 3.16 | 5.70 |
| MIS 16 | 3037.6 | 3039.8 | −441.0 | −412.3 | 78.23 | 12.32 | 111.67 | 21.46 | 32.89 | 11.94 | 3.07 | 4.96 |
| MIS 18 | 3137.8 | 3153.1 | −441.4 | −423.7 | 80.44 | 13.94 | 114.44 | 31.38 | 26.28 | 13.95 | 3.26 | 3.98 |
| Clean Facies | 3201.0 | 3248.0 | −442.5 | −427.7 | 71.78 | 3.79 | 99.91 | 13.39 | 29.03 | 2.42 | 1.94 | 2.40 |
| Dispersed Facies | 3248.0 | 3259.3 | −443.2 | −436.7 | 93.16 | 15.43 | 141.68 | 30.42 | 46.26 | 15.37 | 2.68 | 4.17 |

Finally, Fig. 6 plots the mean equivalent crystal radii for the deep and basal ice, as obtained from preliminary measurements in the field, and compare those to measurements using automatic ice texture analyzers as described in Durand et al. (2009). Reliable measurement of crystals radii in the bottom ice using automatic techniques is hampered by the very large increase of crystal sizes, often spanning several individual thin sections. Only “unconventional” measurements such as, e.g. sonic logging (still in development) might allow us to document these properties further in the future.

5 Discussion

5.1 Indicators of an “undisturbed” paleoclimatic record

In this first section of the discussion, we will demonstrate that some of the clean and dispersed basal ice facies properties appear coherent with a climatic signature unmodified by large-scale refreezing processes. As shown in Fig. 1b, c both the clean and dispersed ice facies display δD values typical of a mild to cold glacial period, with respective

ranges of −427.7 to −442.5 and −436.7 to −443.2 ‰ (Table 1), as would be expected for MIS 20 based on more recent glacials. In the co-isotopic δD – $\delta^{18}\text{O}$ diagram of Fig. 2a, all samples align well with those from the previous climatic cycles, with a slope of 8.5, close to the value of 8.2 for the samples above 3200 m, i.e. in accordance with a meteoric water line. This is very different from the refrozen Vostok lake ice, where the samples were shown to be clearly located on a freezing slope of 4.9, only slightly higher than the theoretical slope calculated from the estimated lake water isotopic value (Souchez et al., 2002a). Also, the d_{excess} values shown in Fig. 2b are within the range of those observed in the more recent glacials, while refreezing processes are known to lower the deuterium excess values (Souchez et al., 2002a; Souchez and Lorrain, 1991). These are first arguments to preclude large-scale refreezing as a plausible process for the bottom-ice formation.

The gas properties of the bottom ice are probably even more indicative of a true climatic signature (Fig. 3a). The total gas content is very stable with a mean value at $0.088 \text{ mL}_{\text{air}} \text{ g}_{\text{ice}}^{-1}$, which is identical to the one obtained for the whole 0–400 ky interval further up in the core (Raynaud et al., 2007). CH₄, N₂O and CO₂ concentrations are also quite

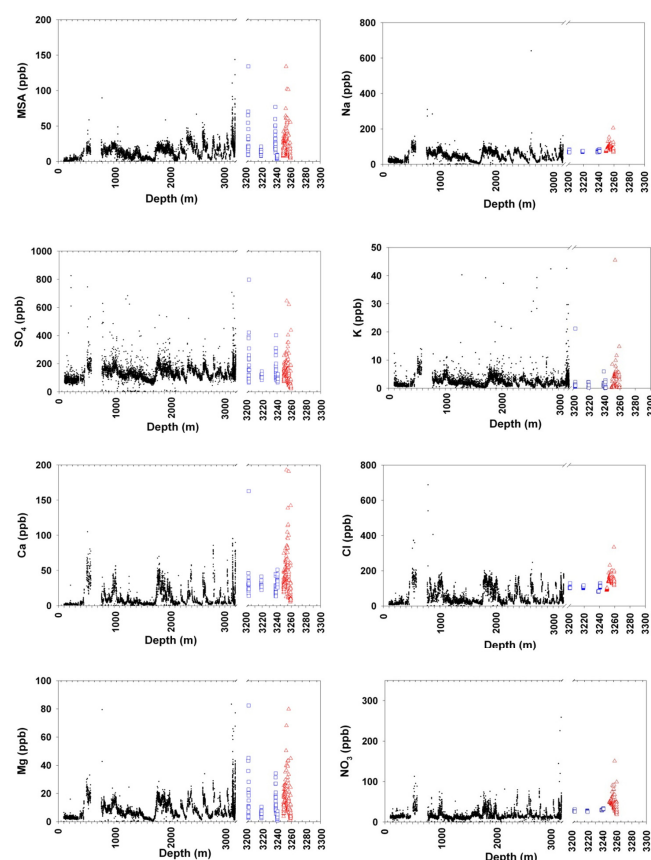


Figure 4. Concentrations (in ppb or ng g^{-1}) of selected chemical species in the clean (open blue squares) and dispersed (open red triangles) basal ice facies of the EPICA Dome C core, as compared to those of the preceding climatic cycles (black dots, courtesy of the EPICA chemical consortium). Resolution is between 5 and 8 cm above 3200 m depth and between 1.5 and 5 cm in the basal ice below 3200 m. Note the change of depth scale below 3200 m.

stable and typical of mild to full glacial conditions (mean values of 417, 247 and 193 ppmv, respectively). $\delta\text{O}_2/\text{N}_2$ (Table S1) are also typical of meteoric ice with values similar to those described in Landais et al. (2012, their Fig. 1, -25°C values). They show no sign of alteration from potential solubility fractionation, as would be expected in the case of significant melting–refreezing processes. Although they show much larger variations, most insoluble dust concentrations also typically lie within the boundaries of a full glacial state (Fig. 3b).

Table 1 gives the mean concentration values of the considered suite of chemical species. A systematic comparison of the mean clean and dispersed ice facies values to those of each of the previous full glacial episodes (with similar δD ranges) shows a very close compatibility, further suggesting that the mean paleoclimatic signal was not modified in the vicinity of the ice–bedrock interface. Indeed, any large-scale regelation process of meteoric ice meltwater would induce

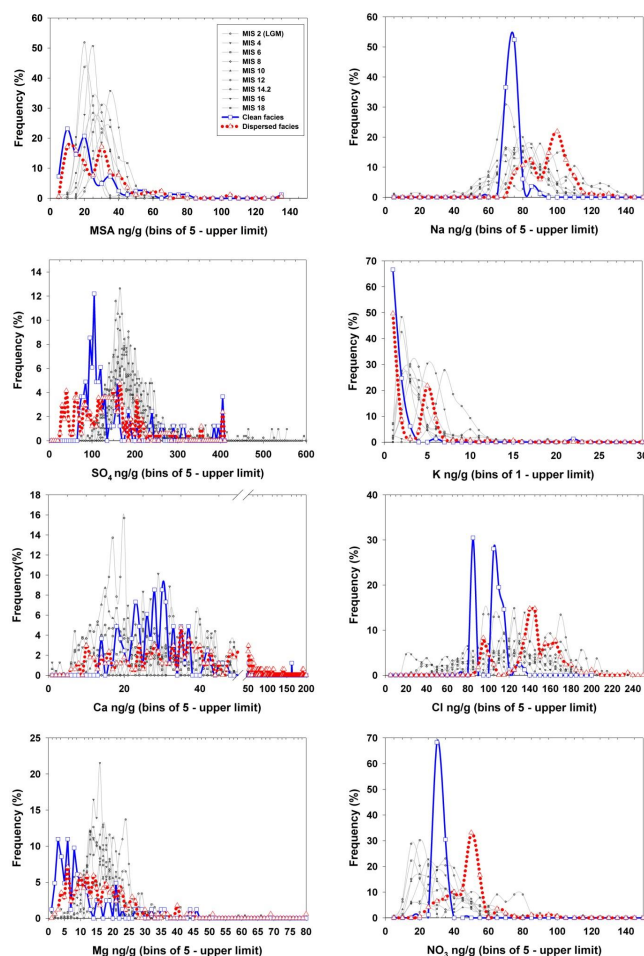


Figure 5. Frequency distribution of concentrations (in bins of 1 or 5 ng g^{-1} or ppb) of selected chemical species in the clean (open blue squares – thick blue solid line) and dispersed (open red triangles – thick red dotted line) basal ice facies of the EPICA Dome C core, as compared to those for the preceding full glacial periods (incremented symbols and thin grey lines – courtesy of EPICA Chemistry Consortium). See text for definition of “full glacials”.

significant departure of the chemical composition (both in terms of total impurity content and of chemical speciation) of the refrozen ice from the initial values present in the meteoric ice. De Angelis et al. (2005, 2004) showed that, in the case of refreezing of the Lake Vostok water, away from any sediment source (their ice type 2), the concentrations were significantly lower than those in meteoric ice, in accordance with the efficient rejection of impurities during freezing at very low rates. Conversely, the upper part of the Vostok lake ice, that is thought to have accreted in a shallow bay upstream of Vostok (ice type 1), shows a total ionic content 5 to 50 times higher than meteoric ice, with a specific signature suggesting contamination from salts originating from deeper sedimentary strata, close to evaporites in composition. Nei-

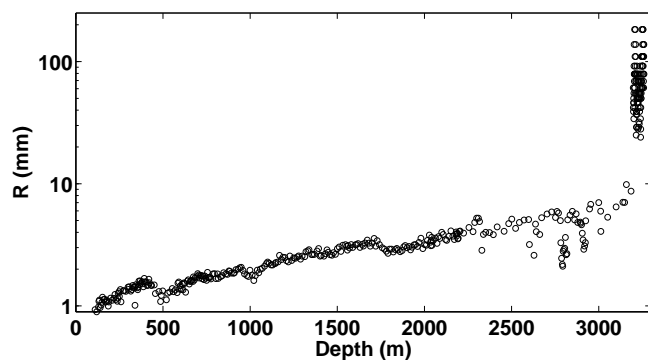


Figure 6. Mean equivalent crystals radii in the basal ice layers of the EPICA Dome C ice core, as compared to measurements in ice above 3200 m depth from Durand et al. (2007). Basal ice measurements are preliminary results obtained using the linear intercept technique “on site”, while the data from above 3200 m were obtained using automatic ice texture analyzers (AITAs – Wang and Azuma, 1999; Russell-Head and Wilson, 2001; Wilen et al., 2003).

ther of these two signatures are seen in the EDC bottom-ice samples.

5.2 Indicators of a “disturbed” paleoclimatic record

There are however some features of the bottom ice that raise questions about its paleoclimatic significance. First of all, as stated above, the presence of visible-solid inclusion aggregates in the lower 12 m could be the result of incorporation processes of sedimentary material at the ice–bedrock interface (Boulton, 1996, 1979; Cuffey et al., 2000; Gow et al., 1979; Gow and Meese, 1996; Herron and Langway, 1979; Holdsworth, 1974; Iverson, 1993; Iverson and Semmens, 1995; Knight, 1997; Koerner and Fisher, 1979; Souchez et al., 1988, 2000b; Tison and Lorrain, 1987; Tison et al., 1993, 1989). Then, a comparison of Fig. 1c and e reveals a strong discrepancy between the EDC δD record and the benthic record stack of Lisiecki and Raimo (2005) prior to 800 ky, with the lack of MIS21 in the EDC profile, which, instead, displays an unusually long glacial period. Furthermore, the $\delta^{18}O_{atm}$ profile of Fig. 1d is also somewhat peculiar in two ways: first it is extremely stable in the bottom ice despite known large fluctuations in the precession and ice volume at the time, to which the $\delta^{18}O_{atm}$ was shown to be very sensitive (Bender, 2002; Dreyfus et al., 2007; Landais et al., 2010), and, second, it displays values continuously close to 0‰, which is generally (but not strictly) more typical of full interglacial rather than full glacial conditions.

Finally, although generally coherent with the previous climatic cycles in terms of mean concentration values, individual chemical species can be considered to be two groups with specific and contrasted chemical distribution (Figs. 4 and 5, Table 1). MSA, SO_4 , Ca and Mg, on the one hand, clearly show increased variability, both in the clean and dispersed ice facies (see left column of Fig. 4 and 1σ values in Table 1), a

trend that seems to initiate in MIS18 already. The frequency distributions in Fig. 5 confirm this variability as compared to previous glacials, with a tendency of both skewing towards lower values for MSA, SO_4 or Mg and showing outliers at higher concentration, especially in the clean ice facies. On the other hand, Na, K, Cl, and NO_3 behave noticeably differently in the clean ice and in the dispersed ice facies (right column in Fig. 4). The clean ice facies (solid line) shows very low variability and narrow frequency peaks in the graphs of Fig. 5, while the dispersed ice facies (dotted line) behaves similarly to the previous glacial, but with a tendency of skewing towards the higher range of concentrations.

5.3 Distribution and relocation of dissolved and solid impurities within ice cores

Ohno et al. (2005) discussed the location and chemical forms of water-soluble salts in ice cores. Initially entrapped in-between the snow grains that will evolve into firn and then ice under increasing metamorphism, these impurities could therefore be found either within the ice crystals themselves, or within the unfrozen liquid that separates the grain boundaries as a result of “premelting” (Rempel et al., 2001, 2002; Wettlaufer, 1999), be it veins, nodes or triple junctions. A common view amongst glaciologists is that because those impurities produce strain-energy within ice grains and because trace acids must exist as acid solutions given their very low eutectic point, they will progressively be forced into grain boundaries as grain growth and recrystallization occur (Glen et al., 1977; Rempel, 2003; Rempel et al., 2001, 2002; Wettlaufer, 1999). Although most of the sulfur atoms appear as sulfuric acid in Antarctic ice (samples were observed at triple junctions of grain boundaries in the early days of scanning electron measurements in ice (Mulvaney et al., 1988)), there has been growing evidence that sulfur compounds also exist as sulfate trapped as inclusions within grains (e.g. Baker and Cullen, 2003). Ohno et al. (2005), using micro-Raman spectroscopy, underline that at shallow depth (185 m) in the Dome Fuji ice core, the fraction of SO_4^{2-} existing as salts within the micro-inclusions exceeded 50 % of the total SO_4^{2-} . Similar fraction values between 30 and 60 % were found for Na^+ , Ca^{2+} and Mg^{2+} in discrete samples spanning the 5.6 to 87.8 ky BP interval.

Relocation of impurities under increasing recrystallization is likely to become important in the deeper part of meteoric ice cores, where the ice temperature gets closer to the pressure melting point (pmp) and the temperature gradient generally increases. One of those relocation processes that has been intensively discussed in the recent years is the mechanism often referred to as “anomalous diffusion” (Rempel, 2003; Rempel et al., 2001, 2002). In this process, it is surmised that, as grains slowly grow and recrystallize within ice sheets, most of the impurity molecules are preferentially excluded from the solid grains and enriched in the melt. As the polycrystalline mixture of ice and premelt liquid solu-

tion flows downwards under gravity at velocity v , it encounters gradual variations in temperature leading to gradients in intergranular concentrations, which, in turn, drive molecular diffusion of solutes relative to the porous ice matrix. The net result is that the bulk impurity profile will move downwards at a rate that differs by a finite “anomalous velocity” v_c from the downward velocity v of the ice itself. A typical modelling case study for the conditions at the location of the GRIP ice core predicts separation of the bulk-impurity profile from the contemporaneous ice by a maximum amount of about 90 cm in the bottom layers (3028 m). However, Barnes and Wolff (2004) suggested that the anomalous velocity calculated in Rempel’s model is largely overestimated, since the latter mainly surmises that all impurities are located at triple junctions. As underlined by these authors, if impurities are transferred at two-grain boundaries, then v_c would be much lower. Also, Ohno et al. (2005), as discussed above, demonstrated that much of these impurities are distributed within the crystal itself, further potentially hampering the “anomalous diffusion” process, as recognized by Rempel (2003). Another important feature of this migration process is that the amplitude of the concentration changes should not be altered, even in the case of asynchronous initial deposition of different species with contrasted concentration levels (Rempel, 2003). It is therefore difficult to invoke anomalous diffusion to explain the contrasts in species concentration variability observed in our bottom ice at EPICA Dome C (see Sect. 4.2).

Another interesting process discussed by Rempel (2005) is the one in which the density difference between inter-crystalline interstitial water (premelt) and ice produces a hydraulic gradient that drives a downward liquid flow. When the temperature rises towards the glacier bed, the associated permeability increase leads to more rapid fluid transport, internal melting supplying the changing flow. Although the author shows that, in the specific case where the lower region of the glacier floats on a subglacial reservoir, a reduction in the hydraulic gradient results from surface energy effects and causes a decreasing transport rate in the lower few tens of centimetres, the process mentioned above provides a potential mechanism for downward migration of the chemical compounds accumulated in the premelt layer as recrystallization at high temperature proceeds.

Finally, it is also worth looking at the few detailed studies on impurity distribution within the accreted lake ice of Lake Vostok (de Angelis et al., 2004, 2005). Although the form (solid vs. dissolved) and origin of these impurities might differ from those found in meteoric ice above, both ice types (bottom meteoric ice at EDC and accreted ice at Vostok) were submitted to intense recrystallization at high temperatures ($> -5^\circ\text{C}$), potentially involving impurity relocation. Indeed, a strong 10-fold increase of grain size is observed in the EDC bottom ice (Fig. 6), and huge increases (several tens of cm in size-crystals) are reported at Vostok (Montagnat et al., 2001). It is interesting to note that the high-resolution spa-

tial distribution of impurities in both EDC (bottom) and Vostok (lake) ice present striking similarities. Indeed, fine-scale (1 cm) analyses of ion concentration in accreted ice samples at Vostok (e.g. Fig. 5 in de Angelis et al., 2004) show that Cl, Na, F and NO_3 have a uniform distribution throughout the samples, while SO_4 , Ca and Mg are much more heterogeneous. This is clearly the behaviour we underlined in our EDC bottom ice (Figs. 4 and 5): much higher variability in the basal ice than in the meteoric ice above, and much higher variability for SO_4 , Ca, Mg and MSA (ion absent in Vostok refrozen ice due to lake water concentration) than for Na, K, Cl and NO_3 in both the clean and dispersed basal ice facies. In the case of the Vostok accreted ice, de Angelis et al. (2005) observed that Cl, Na and K are incorporated within bubble-shaped structures, very likely brine micro-pockets refrozen during the core extraction, while SO_4 , Ca and Mg are present in aggregates of insoluble material (initially suspended in the lake water), all impurities being originally randomly distributed within the unconsolidated frazil ice lattice. These authors then surmise that, as consolidation, grain growth and re-crystallization occur at high temperature (-3°C), brine micro droplets containing soluble salt ionic species like Cl^- , Na^+ or K^+ are not relocated and remain homogeneously distributed throughout the ice lattice, while ions associated to fine solid salt particles, are excluded and gathered with other mineral particles in inclusions of increasing sizes, leading to a greater heterogeneity. Although SO_4 salts and associated species clearly could not initially exist as a suspension in lake water in the EDC case (where refreezing of a water body is inconsistent with the isotopic and gas data sets (see Sect. 4.1. above)), they may be formed through in situ chemical reactions and a similar relocation process of atmospheric inputs under recrystallization could have been at work (see sect. 5.4. below).

5.4 Scenarios for the build-up and evolution of the EPICA deep and basal ice

5.4.1 Mixing?

We saw in the previous sections that some of the properties of the EDC bottom ice are consistent with a pristine paleoclimatic record, while other properties raise some suspicion. We also demonstrated that significant net refreezing of a water body at the bottom of the ice sheet can be discarded. Another set of processes that were shown to alter the basal ice properties is mixing or folding under enhanced deformation close to the ice–bedrock interface (Souchez, 1997; Souchez et al., 1995b, 1998, 2003). Among the anomalies in EDC bottom-ice properties, the stability of the δD profile for an unusual period of time, if we trust the EDC timescale and compare our data to the Lisiecki and Raymo benthic record (Fig. 1c, e), is probably the most prominent. Homogenization through mixing is a process that was invoked by Souchez et al. (2002a, b) to explain the isotopic properties of the 3400–

3538 m Vostok depth interval, just above the meteoric-lake-ice interface. They indeed show that the δD values are there bracketed in a tight range corresponding to mean values between glacial and interglacial, and that the deuterium excess variability is also strongly reduced. This was supported by the ionic signature showing a narrow range of concentrations corresponding to ice formed under mild glacial conditions. If this was the case for the EDC bottom ice, we should expect (from the comparison of Fig. 1c and e) that the bottom ice shows mean isotopic values between those of MIS20 and MIS21 in Fig. 2b. However, the bottom ice is truly of glacial signature. Also, samples from the basal ice span the whole glacial deuterium excess range.

Mixing with a local isotopic end member inherited from a previous or initial ice sheet configuration is also unlikely. It was only described for basal ice condition largely below the pmp (see Sect. 1) and generally showed contrasting properties between the present-day ice sheet ice and the local end member, with a whole range of intermediate values in the mixing zone.

5.4.2 Stretching?

If mixing is therefore improbable at EDC, another mechanical way of explaining the abnormal length of MIS20 is relative vertical stretching under changing stress conditions, i.e. alteration of the stratigraphic timescale. Although, given the location chosen for the EPICA Dome C drilling, stress conditions should be (and are) essentially those of vertical uniaxial compression, Durand et al. (2008) indicate that the fabrics in layers of larger mean crystal sizes (about 6 mm) below 2850 m show signs of dispersion of the strong single maximum (which is the rule below 1500 m depth) along a weak vertical girdle. These changes might be the sign of evolving stress conditions near the bottom of the ice sheet, and were recently interpreted so, to explain anomalous flow below 2700 m (Dreyfus et al., 2007) and reworking of sulphate spikes below 2800 m under increased recrystallization (Traversi et al., 2006, 2009).

As seen on the large-scale map of the bedrock elevation in the vicinity of the EDC drilling site (Remy and Tobacco, 2000, their Fig. 4), the ice core bottom location sits at ca. 70 m above sea level, on the eastern flank (200–400 m a.s.l. ridge) of a major S–N trending subglacial valley, with a 400 m a.s.l. ridge 15 km across, on the western flank of the valley. The bottom of the central part of the valley is at ca. 50 m below sea level. The next 400 m deep subglacial valley lies about 20 km further to the east.

In Fig. 7, we schematically show what might be the impact of a confining bedrock topography consisting of elongated valleys about 20 km wide and 200–400 m deep (Rémy and Tobacco, 2000) on the stress field and the ice fabric in the bottom ice of EPICA DC. As the ice sinks passed the crests of the subglacial valleys, lateral compression on the sides of the valley will progressively combine with the vertical uni-

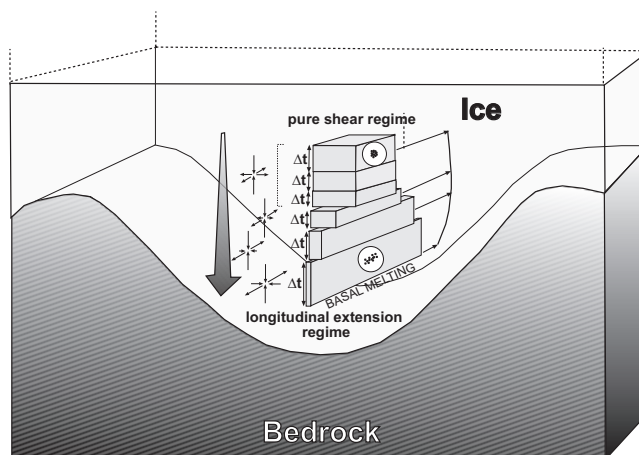


Figure 7. Schematic illustration of the hypothesized impact of the confining bedrock topography (bedrock valleys about 20 km wide and 200–400 m deep – from Remy and Tobacco, 2000) on the stress regime, layer thickness and ice fabric patterns in the bottom ice of EPICA Dome C. Vertical stretching is accommodated by basal melting and/or along sub-glacial valley flow. For clarity, this illustration enhances the process so that absolute annual layer thickness increases downwards. A milder effect would only result in a decrease of the thinning rate (see text for details).

axial compression. The resulting stress field will therefore transition from uniaxial vertical compression to longitudinal extension, as illustrated by the 3-D arrows in the central part of the drawing of Fig. 7. The associated change in fabrics will be from a vertical single maximum to a vertical girdle fabric, in a plane parallel to the subglacial valley sides. This new pattern might be the one already suggested in the discretely changing fabrics described by Durand et al. (2008) below 2800 m. Because the principal stress transverse to the subglacial valley slowly shifts from extensional to compressive, the result could be a relative vertical stretching of individual accumulation layers, depending on the intensity of the principal extension along the valley axis. It is however not possible, with the data at hand, to demonstrate whether this relative vertical stretching results in an absolute increase of annual layer thickness (as shown in Fig. 7) or if it only results in a decrease of the thinning rate. In this configuration, one must of course consider a 3-D geometry, in which the vertically stretched ice can be moved away from the drill location. Part of it can be melted at the ice–bedrock interface where the ice is at the pressure-melting point, and the over-deepening of the longitudinal valleys seen in Fig. 3 of Rémy and Tobacco (2000) could also provide an escape route for the ice.

5.4.3 Enhanced recrystallization and small-scale chemical sorting

In the dynamic context described above (Sect. 5.4.2), and relying on our multiparametric results, we can now propose a

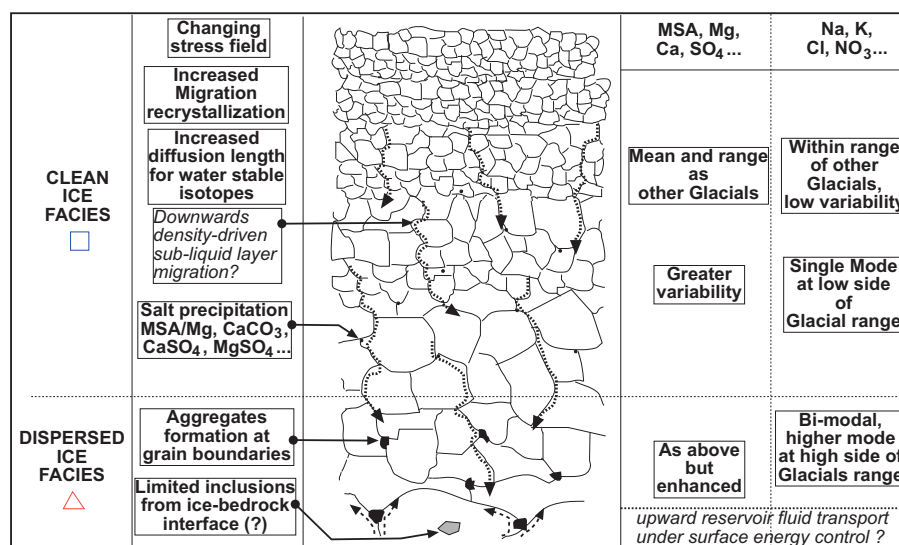


Figure 8. Sketch of potential chemical sorting effects during enhanced migration recrystallization processes under a changing stress field, close to the pressure melting point, in the clean and dispersed basal ice facies of EPICA Dome C. Processes in italic/dotted arrows are hypothetical (see text for details).

plausible scenario for the evolution of the properties of our clean and dispersed basal ice facies at EPICA Dome C, as illustrated in Fig. 8. A changing stress field and the high temperatures, close to the pmp, will trigger sustained migration recrystallization within the bottom layers. Mean crystal size values (up to more than 10 cm) plotted in Fig. 6 are undisputable proof that recrystallization is indeed very active there. This process will tend to relocate the impurities at grain boundaries and contribute to the build-up of aggregates. Note that Raisbeck et al. (2006) already invoked the formation of aggregates to explain abnormal spikes in ^{10}Be in the basal ice. Increasing water content in the premelt layer might also slowly initiate downward density-driven migration of the water and of some of the associated impurities. This however, as our data set shows, will only be revealed in a high resolution chemistry approach, since it will not significantly affect the mean concentration values for a given climatic period, but more the frequency distribution within the observed concentration range. It will also behave differently, depending on the species. Detailed SEM (scanning electron microscope) and XRF (X-ray fluorescence) micro-probe elemental analyses of individual aggregates inside the EDC dispersed basal ice facies are described elsewhere and provide further insights in the potential processes at work and environmental implications (de Angelis et al., 2013). They reveal that CaCO_3 and CaSO_4 are common within these aggregates. These compounds could then be either newly precipitated salts (as observed concentrations are compatible with saturation for, e.g. CaSO_4 given estimated vein sizes at those ambient temperatures) or pre-existing solid particles, that were initially present inside the crystals (Ohno et al., 2005). SO_4 , Ca, Mg and MSA (which can also be associated with salts,

Ohno et al., 2005) mean concentrations in the clean and the dispersed basal ice facies will therefore remain within the range of other glacials, but their spatial distribution at the high-resolution scale of sampling will show much greater variability than in meteoric ice as shown above (Figs. 4, 5 and 8, right column).

As discussed above, the other group of species (Na, Cl, K, NO_3) shows two important features in the frequency distribution of Fig. 5 (right column): (a) although the whole data set is spanning the range of the previous glacials, the concentration mode is lower for the clean ice facies and higher for the dispersed ice facies and (b) the frequency distribution in the basal ice facies is generally single-modal and narrow, while it is bi-modal in the dispersed ice facies with the first mode in the basal ice facies range and the second mode skewed towards the high side of the range observed in other glacials. The contrast in concentration level between the clean ice facies and the dispersed ice facies could simply reflect the slightly colder conditions (thus higher impurity content) at the time the ice of the dispersed basal facies was formed at the surface of the ice sheet, as suggested by the lower δD values compared to the clean ice facies (Fig. 1b). Although this contrast is less obvious for the first group of chemical compounds, it might have been over-written by invoked aggregation and new in situ precipitation processes. Alternatively, the observed contrast in behaviour of Na, Cl, K, NO_3 between the clean and dispersed ice facies might reflect the signature of the premelt migration process as theoretically proposed by Rempel (2005). These species would indeed remain in the dissolved state within the premelt layer, and eventually partly and more easily migrate downwards, resulting in the left skewing mode in the clean ice facies

and the bimodal distribution in the dispersed ice facies (low concentration mode corresponding to the remaining fraction in crystals as salts micro-inclusions and high concentration mode to the fraction that migrated in the premelt). Note that the process of upward pulling of liquid from the underlying reservoir discussed by Rempel (2005), if it exists, provides a means to prevent expulsion of the premelt from the basal ice, and therefore preservation of this bi-modal frequency distribution. Basal melting would potentially counteract this effect but the two basal ice facies would then migrate upwards into the ice column. Unfortunately, as underlined before, the available data set is missing the lower 6–15 m of the basal ice section to the ice–bedrock interface, where further arguments might have been found to (in-) validate this premelt migration hypothesis.

The large inclusions visible in the bottom 12 metres of basal ice are principally located at grain boundaries. Theoretical considerations from Alley et al. (1986, Eq. 21) suggest a high velocity ice grain boundary migration regime with decoupling of the grain boundaries from the particle aggregates because of their relatively large sizes and very low volume fraction. However, as underlined by these authors, this is probably no more valid for the “warm” (EDC bottom) ice, in a full migration recrystallization process, where the increased water content in the vein network will favour Ostwald ripening as the temperature of the ice-impurity system rises above the melting point of the impure grain boundaries. Another feature to consider here is that the particle aggregates might also behave very differently from single particles in terms of drag force on the grain boundaries. Also, as discussed in de Angelis et al. (2013), the significant contribution of organic compounds (such as exopolymeric substances – EPS) to the impurity load might also strongly affect the inclusion/grain boundary geometrical relationships.

5.4.4 Water isotopes, gases and dust

We focused until now on a plausible explanation for the peculiarities of the chemical signature of our two basal ice facies at EDC. How do the water isotopes signature, gas and dust properties fit into the proposed mechanism? Although the water co-isotopic signature of our basal ice facies does not show large-scale signs of modification, the recent work of Pol et al. (2010) suggests that it might not be the case at the crystal size scale, thereby providing some independent support to the interpretation of our chemical data set. These authors indeed used high-resolution (cm scale) δD measurements to depict abnormal isotopic diffusion which they attributed to water circulation at grain boundaries (premelting) for large crystals which spent more than 200 000 years at temperatures $> -10^\circ\text{C}$. The diffusion length diagnosed from the data is about twice as large (40 cm) as expected from solid state diffusion in ice, and it is also suggested that the process might start as early as in MIS 11 (Pol et al., 2011).

Why would the relocation process invoked for the chemical impurities not show up in the total air content or the CH_4 and CO_2 concentrations? First of all, it should be noted that the resolution of our gas data sets is much lower than the one we achieved for the chemical species. Also, one should remember that the gas molecules are exclusively present as clathrates at these depths and little is known on the behaviour of those during small-scale phase changes under large overburden pressures. If the glacial MIS20 “stretching” hypothesis is valid, it is not surprising to observe a stable $\delta^{18}\text{O}_{\text{atm}}$ signal. Landais and Dreyfus (2010) provide an in depth analysis of the potential drivers for the millennial and orbital variations of $\delta^{18}\text{O}_{\text{atm}}$ and show the strong impact of Northern Hemisphere monsoon activity on the observed values, in response to precessional and millennial shifts of the Intertropical Convergence Zone (ITCZ). Intervals where $\delta^{18}\text{O}_{\text{atm}}$ is close to 0 ‰ correspond in that context to episodes where precession favours warm Northern Hemisphere summers with a strong East-Asian monsoon. In Fig. 1f, we plotted the values for the integrated summer insolation at 30°N , for various thresholds τ , as calculated by Huybers (2006). This integrated summer insolation can be defined as the sum of the diurnal average insolation on days exceeding a specified flux threshold (τ). As can be seen from the comparison between Fig. 1f and d, high values of $\delta^{18}\text{O}_{\text{atm}}$ concur with high integrated summer insolation associated with very high diurnal average insolation thresholds (e.g. for $\tau = 450$ (green curve) to 500 (red curve) Watt m^{-2} in Fig. 1f), which is the case for our basal ice sequence. This relationship is enlarged in Fig. 9a, where one can clearly see that maxima in $\delta^{18}\text{O}_{\text{atm}}$ are well coupled to maxima in integrated summer insolation (to the exception of a missing peak around 750 ky). It can also be suggested that larger $\delta^{18}\text{O}$ amplitudes correspond to larger summer insolation values and vice versa, with a threshold around roughly 2 GJ. In Fig. 9a we attempted to use the synchronicity of small-scale oscillations of the $\delta^{18}\text{O}_{\text{atm}}$ signal (however well above the precision of measurements -0.015‰), to the summer insolation one (tie points 1 and 2 in Fig. 9a) to derive the amount of stretching of the basal ice sequence. This produces a factor of about 2, which allowed us to reconstruct a new timescale for the basal ice, assuming linear stretching also applying to the bottom ice, for which $\delta^{18}\text{O}_{\text{atm}}$ are not available. Unfortunately, this does not resolve the discrepancy with the Lisiecki and Raymo curve (Fig. 9b), and suggests that the amount of stretching is probably much larger, with an initial time frame for the basal ice of only about 10 000 years. To build our 60 m of basal ice sequence in ca. 10 000 years would require an “in situ” annual layer thickness of 6 mm, which is 10 times the value observed during the previous glacial, following the recently published AICC2012 climate record (Bazin et al., 2013, Supplement). This seems too extreme, and suggests stretching might have been supplemented by other processes such as dynamical thickening in the lee of bedrock obstacles or stacking up of several glacials, with missing interglacials. The latter is how-

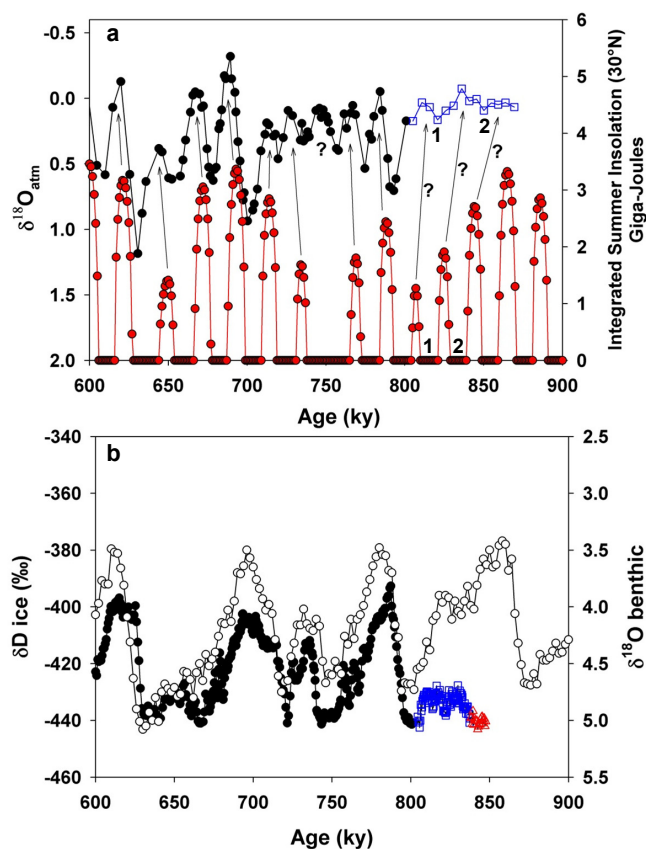


Figure 9. Attempting to reconstruct the timescale for the basal ice sequence: (a) zoom on the $\delta^{18}\text{O}_{\text{atm}}$ curve vs. integrated summer insolation at 30°N (see Fig. 1e) and (b) comparison of the benthic $\delta^{18}\text{O}$ curve (open circles) to the EPICA $\delta\text{D}_{\text{ice}}$ profile (black dots), where the basal ice timescale was linearly “compressed” using tie points 1 and 2 in (a) (see text for details).

ever unlikely, since interglacial ice is usually harder to deform due to lower impurity content and larger crystal size (Dahl-Jensen et al., 2013). Finally, as demonstrated in de Angelis et al. (2013), the detailed analysis of individual inclusions supports the occurrence of in situ bacterial activity. To our knowledge, it is not known so far if these might have potential impact on the $\delta^{18}\text{O}_{\text{atm}}$ of the neighbouring gas phase. It is however unlikely that it might be significant given the observed low CO_2 mixing ratio (Fig. 3a), in line with atmospheric values at glacial times.

Despite the very poor resolution of the dust record in our bottom ice the large variability of the data within the glacial range could also result from our increased relocation scheme. Moreover, below 2900 m, a significant shift of particle size towards large diameters is in agreement with the formation of aggregates.

6 Conclusions

We used a multiparametric approach to discuss the plausibility of recovering an unaltered paleoclimatic signature from the basal ice of the EDC ice core. We showed that some of the data (δD values, total air content, gas composition, dust content, mean chemical species concentrations) suggest a pristine meteoric glacial signature while other data (length of the glacial, $\delta^{18}\text{O}_{\text{atm}}$, visible inclusions, variability of the chemical species distribution) suggest mechanical and compositional alteration of the bottom ice. Ice stable isotopes and total air content rule out large-scale refreezing processes of a water reservoir as the origin for the bottom ice. Mixing, be it internally (as in Vostok MIS11) or with a local ice remnant of previous or initial ice sheet configuration (as in GRIP and Dye-3) can be equally discarded.

Using a new high resolution data set for selected chemical species in the basal EDC ice and remote sensing information on the general setting of the Dome C area, we propose a mechanism in which the confining bedrock topography contributes to a downward change in the stress field from uniaxial vertical compression to longitudinal extension along the valley axis. This stress configuration change results in a potential relative vertical stretching of the ice layers, which explains the abnormal length of MIS20. Combined with an ice temperature close to the pmp it also favours rapid migration recrystallization, as witnessed by the large increase in grain size. This, in turn, induces relocation of impurities, with accumulation of newly formed salts and already existing solid particles in the premelt layer, forming aggregates. Those become visible about 12 m above the bottom of the core and increase in size and number downwards. The basal inclusions thus mainly consist of reworked existing material; they do not represent the incorporation of allochthonous material from the ice–bedrock interface. However some potential candidates for the latter (large, single, mineral inclusions) were detected in the last meter layer (de Angelis et al., 2013). Although the mean concentration values were not significantly different from those observed in the previous full glacial periods, some chemical sorting is apparent, especially for those species that are not involved in salt formation. We suggest this might result from a slow process of downward migration of the premelt layer under the hydraulic gradient resulting from the density difference between ice and interstitial water, although the lack of data from the last 6–15 m to the ice–bedrock interface prevents us from further validating this hypothesis. The ice isotopic and gas properties are apparently not affected by these small-scale processes that, however, only become detectable at high-resolution sampling (sub-crystal size), where they are involved in smoothing processes. The apparent discrepancy in the $\delta^{18}\text{O}_{\text{atm}}$ signal is resolved if one considers potential stretching of a glacial time span during which precession favours warm Northern Hemisphere summers, as happened temporarily in each of the previous glacial isotopic stages.

We conclude that the paleoclimatic signal is only marginally affected in terms of global ice properties at the bottom of EPICA Dome C, but that the timescale was considerably distorted by mechanical stretching due to the increasing influence of the subglacial topography. It is interesting to note that MIS18 already shows signs of isotopic smoothing, chemical relocation and increased variability for the species involved in salt formation (MSA, SO₄, Mg and, in a lesser extent Ca), before the timescale (EDC3) got significantly distorted. Along the same line the anomalous flow detected below 2700m, that led to the change from the EDC2 to the EDC3 timescale, might already find its roots in this subglacial topography distortion, although possible changes in the Dome position with time need also to be considered (e.g. Urbini et al., 2008). Many interior ice divides are indeed migrating today, and this could also be the case for the EDC location. Given the rough bed topography, it takes a migration of only a few ice thicknesses to change the bedrock elevation by ca. 200 m. The basal ice may therefore have experienced vertical stretching due to flow from the bedrock ridge to the current valley position, with recent migration of the divide at the top. Today, lively discussions exist and preliminary actions are undertaken within the ice core community to select a suitable location for a new deep drilling targeting the “oldest ice” (above 1 million years old, IPICS, 2009). Our work shows that the location of the EDC ice core on the flank of a valley-type subglacial topography has considerably affected the inference of deep timescales. We conclude that the retrieving of reliable paleoclimatic signals down to a few metres from the ice–bedrock interface would probably be thinkable on a flat monotonic bedrock, for distances several times the local ice thickness, although small-scale reworking of some of the proxies should be expected. It is however not clear yet why the gas content and composition is so well preserved at EDC, and not at other deep basal ice location. The presence of a liquid water layer at the interface might partly explain that discrepancy, although this could not be verified here.

Future work on the EPICA DC bottom ice will involve high resolution gas measurements in selected areas and an in-depth analysis of the crystallographic properties below 3200 m. Hopefully, these will allow us to validate and refine the general mechanism discussed here.

The Supplement related to this article is available online at doi:10.5194/tc-9-1633-2015-supplement.

Acknowledgements. This work is a contribution to the European Project for Ice Coring in Antarctica (EPICA), a joint European Science Foundation/European Commission (EC) scientific programme, funded by the EU (EPICA-MIS) and by national contributions from Belgium, Denmark, France, Germany, Italy, The

Netherlands, Norway, Sweden, Switzerland and the UK. The main logistic support at Dome C was provided by IPEV and PNRA. The authors wish to warmly thank B. Hubbard and two anonymous referees for their constructive comments on the “Discussion” version of this manuscript, and D. Raynaud and F. Parrenin for valuable discussions.

Edited by: M. Schneebeli

References

- Alley, R. B., Perepezko, J. H., and Bentley, C. R.: Grain growth in polar ice, I. Theory, *J. Glaciol.*, 32, 415–424, 1986.
- Baker, I. and Cullen, D.: SEM/EDS observations of impurities in polar ice: artefacts or not?, *J. Glaciol.*, 49, 184–190, 2003.
- Bazin, L., Landais, A., Lemieux-Dudon, B., Toyé Mahamadou Kele, H., Veres, D., Parrenin, F., Martinerie, P., Ritz, C., Capron, E., Lipenkov, V., Loutre, M.-F., Raynaud, D., Vinther, B., Svensson, A., Rasmussen, S. O., Severi, M., Blunier, T., Leuenberger, M., Fischer, H., Masson-Delmotte, V., Chappellaz, J., and Wolff, E.: An optimized multi-proxy, multi-site Antarctic ice and gas orbital chronology (AICC2012): 120–800 ka, *Clim. Past*, 9, 1715–1731, doi:10.5194/cp-9-1715-2013, 2013.
- Bender, M. L.: Orbital tuning chronology for the Vostok climate record supported by trapped gas composition, *Earth Planet. Sci. Lett.*, 204, 275–289, 2002.
- Boulton, G. S.: Processes of erosion on different substrata, *J. Glaciol.*, 23, 15–38, 1979.
- Boulton, G. S.: Theory of glacial erosion, transport and deposition as consequence of subglacial sediment deformation, *J. Glaciol.*, 42, 43–62, 1996.
- Cuffey, K., Conway, H., Gades, A., Hallet, B., Lorrain, R., Severinghaus, J. P., Steig, E., Vaughn, B., and White, J.: Entrainment at cold glacier beds, *Geology*, 28, 351–354, 2000.
- Dahl-Jensen, D., Albert, M. R., Aldahan, A., Azuma, N., Balslev-Clausen, D., Baumgartner, M., Berggren, A.-M., Bigler, M., Binder, T., Blunier, T., Bourgeois, J. C., Brook, E. J., Buchardt, S. L., Buizert, C., Capron, E., Chappellaz, J., Chung, J., Clausen, H. B., Cvijanovic, I., Davies, S. M., Ditlevsen, P., Eicher, O., Fischer, H., Fisher, D. a., Fleet, L. G., Gfeller, G., Gkinis, V., Gogineni, S., Goto-Azuma, K., Grinsted, A., Gudlaugsdottir, H., Guillevic, M., Hansen, S. B., Hansson, M., Hirabayashi, M., Hong, S., Hur, S. D., Huybrechts, P., Hvidberg, C. S., Iizuka, Y., Jenk, T., Johnsen, S. J., Jones, T. R., Jouzel, J., Karlsson, N. B., Kawamura, K., Keegan, K., Kettner, E., Kipfstuhl, S., Kjær, H. a., Koutnik, M., Kuramoto, T., Köhler, P., Laepple, T., Landais, A., Langen, P. L., Larsen, L. B., Leuenberger, D., Leuenberger, M., Leuschen, C., Li, J., Lipenkov, V., Martinerie, P., Maselli, O. J., Masson-Delmotte, V., McConnell, J. R., Miller, H., Mini, O., Miyamoto, A., Montagnat-Rentier, M., Mulvaney, R., Muscheler, R., Orsi, a. J., Paden, J., Panton, C., Pattyn, F., Petit, J.-R., Pol, K., Popp, T., Possnert, G., Prié, F., Prokopiou, M., Quiquet, A., Rasmussen, S. O., Raynaud, D., Ren, J., Reutenauer, C., Ritz, C., Röckmann, T., Rosen, J. L., Rubino, M., Rybak, O., Samyn, D., Sapart, C. J., Schilt, A., Schmidt, a. M. Z., Schwander, J., Schüpbach, S., Seierstad, I., Severinghaus, J. P., Sheldon, S., Simonsen, S. B., Sjolte, J., Solgaard, A. M., Sowers, T., Sperlich, P., Steen-Larsen, H. C., Steffen, K., Steffensen, J.-P., Stein-

- hage, D., Stocker, T. F., Stowasser, C., Sturlvik, A. S., Sturges, W. T., Sveinbjörnsdóttir, A., Svensson, A., Tison, J.-L., Uetake, J., Valleslonga, P., Van der Wal, R. S. W., van der Well, G., Vaughn, B. H., Vinther, B., Waddington, E., Wegner, A., Weikusat, I., White, J. W. C., Wilhems, F., Winstrup, M., Witrant, E., Wolff, E. W., Xiao, C., and Zheng, J.: Eemian interglacial reconstructed from a Greenland folded ice core, *Nature*, 493, 489–494, 2013.
- de Angelis, M., Petit, J.-R., Savarino, J., Souchez, R., and Thieme, M. H.: Contributions of an ancient evaporitic-type reservoir to subglacial Lake Vostok chemistry, *Earth Planet. Sci. Lett.*, 222, 751–765, 2004.
- de Angelis, M., Morel-Fourcade, M.-C. B., J.-M., Susini, J., and Duval, P.: Brine micro-droplets and solid inclusions in accreted ice from Lake Vostok (East Antarctica), *Geophys. Res. Lett.*, 32, L12501, doi:10.1029/2005GL022460, 2005.
- de Angelis, M., Tison, J.-L., Morel-Fourcade, M.-C., and Susini, J.: Micro-investigation of EPICA Dome C bottom ice: Evidence of long term *in situ* processes involving acid-salt interactions, mineral dust and organic matter, *Quaternary Sci. Rev.*, 78, 248–265, 2013.
- Delmonte, B., Andersson, P. S., Haqnsen, M., Schöberg, H., Petit, J.-R., Basile-Doelsch, I., and Maggi, V.: Aeolian dust in East Antarctica (EPICA-Dome C and Vostok): Provenance during glacial ages over the last 800 kyr, *Geophys. Res. Lett.*, 35, L07703, doi:10.1029/2008GRL033382, 2008.
- Dreyfus, G. B., Parrenin, F., Lemieux-Dudon, B., Durand, G., Masson-Delmotte, V., Jouzel, J., Barnola, J.-M., Panno, L., Spahni, R., Tisserand, A., Siegenthaler, U., and Leuenberger, M.: Anomalous flow below 2700 m in the EPICA Dome C ice core detected using $\delta^{18}\text{O}$ of atmospheric oxygen measurements, *Clim. Past*, 3, 341–353, doi:10.5194/cp-3-341-2007, 2007.
- Durand, G., Svensson, A., Persson, A., Gagliardini, O., Gillet-Chaulet, F., Sjolte, J., Montagnat, M., and Dahl-Jensen, D.: Evolution of the texture along the EPICA Dome C ice core, *Proceedings of the 2nd International Workshop on Physics of Ice Core records (PICR-2)*, Hokkaido University, Sapporo, Japan, Institute of Low Temperature Science, 2009.
- EPICA_Community_members: Eight glacial cycles from an Antarctic ice core, *Nature*, 429, 623–628, 2004.
- Glen, J. W., Homer, D. R., and Paren, J. G.: Water at grain boundaries: its role in the purification of temperate glacier ice, *Int. Assoc. Hydrogeol.*, 118, 263–271, 1977.
- Goodwin, I. D.: Basal ice accretion and debris entrainment within the coastal ice margin, Law Dome, Antarctica, *J. Glaciol.*, 39, 157–166, 1993.
- Gow, A. J. and Meese, D. A.: Nature of basal debris in the GISP2 and Byrd ice cores and its relevance to bed processes, *Ann. Glaciol.*, 22, 134–140, 1996.
- Gow, A. J., Epstein, S., and Sheehy, W.: On the origin of stratified debris in ice cores from the bottom of the Antarctic Ice Sheet, *J. Glaciol.*, 23, 185–192, 1979.
- Herron, S. and Langway, C.: The debris-laden ice at the bottom of the Greenland ice-sheet, *J. Glaciol.*, 23, 193–207, 1979.
- Holdsworth, G.: Meserve Glacier, Wright Valley, Antarctica – part I: Basal processes, no. 37, Institute of Polar Studies, The Ohio State University Research Foundation, Columbus, 1974.
- Hubbard, B., Cook, S., and Coulson, H.: Basal ice facies: a review and unifying approach, *Quat. Sc. Rev.*, 28, 1956–1969, 2009.
- Huybers, P.: Early Pleistocene glacial cycles and the integrated summer insolation forcing, *Science*, 313, 508–511, 2006.
- International Partnerships in Ice Core Sciences: IPICS White papers, www.pages-igbp.org/ipics/whitepapers.html, 2009.
- Iverson, N. R.: Regelation of ice through debris at glacier beds: Implications for sediment transport, *Geology*, 21, 559–562, 1993.
- Iverson, N. R. and Semmens, D.: Intrusion of ice into porous media by regelation: A mechanism of sediment entrainment by glaciers, *J. Geophys. Res.*, 100, 10219–10230, 1995.
- Jouzel, J., Petit, J. R., Souchez, R., Barkov, N., Lipenkov, V., Raynaud, D., Stievenard, M., Vassiliev, N., Verbeke, V., and Vimeux, F.: More than 200 meters of lake ice above subglacial lake Vostok, Antarctica, *Science*, 286, 2138–2141, 1999.
- Jouzel, J., Masson-Delmotte, V., Cattani, O., Dreyfus, G., Falourd, S., Hoffmann, G., Minster, B., Nouet, J., Barnola, J.M., Chappellaz, J., Fischer, H., Gallet, J.C., Johnsen, S., Leuenberger, M., Loulergue, L., Luethi, D., Oerter, H., Parrenin, F., Raisbeck, G., Raynaud, D., Schilt, A., Schwander, J., Selmo, E., Souchez, R., Spahni, R., Stauffer, B., Steffensen, J.-P., Stenni, B., Stocker, T.F., Tison, J.-L., Werner, M., and Wolff, E. W.: Orbital and Millennial Antarctic Climate Variability over the Past 800 000 Years, *Science*, 317, 5839, doi:10.1126/science.1141038, 2007.
- Knight, P. G.: The basal ice layer of glaciers and ice sheets, *Quat. Sci. Rev.*, 16, 975–993, 1997.
- Koerner, R. M. and Fisher, D. A.: Discontinuous flow, ice texture, and dirt content in the basal layers of the Devon Island Ice Cap, *J. Glaciol.*, 23, 209–221, 1979.
- Lambert, F., Delmonte, B., Petit, J.-R., Bigler, M., Kaufmann, P. R., Hutterli, M. A., Stocker, T. F., Ruth, U., Steffensen, J. P., and Maggi, V.: Dust-Climate couplings over the past 800 000 years from the EPICA Dome C ice core, *Nature*, 452, 616–619, doi:10.1038/nature06763, 2008.
- Landais, A., Dreyfus, G., Capron, E., Masson-Delmotte, V., Sanchez-Goni, M. F., Desprat, S., Hoffmann, G., Jouzel, J., Leuenberger, M., and Johnsen, S.: What drives the millennial and orbital variations of $\delta^{18}\text{O}_{\text{atm}}$?, *Quaternary Sci. Rev.*, 29, 235–246, 2010.
- Landais, A., Dreyfus, G., Capron, E., Pol, K., Loutre, M. F., Raynaud, D., Lipenkov, V. Y., Arnaud, L., Masson-Delmotte, V., Paillard, D., Jouzel, J., and Leuenberger, M.: Towards orbital dating of the EPICA Dome C ice core using $\delta\text{O}_2 / \text{N}_2$, *Clim. Past*, 8, 191–203, doi:10.5194/cp-8-191-2012, 2012.
- Lefebvre, E., Ritz, C., Legrésy, B., and Possenti, P.: New temperature profile measurement in the EPICA Dome C borehole, *Geophysical Research Abstracts*, EGU General Assembly 2008, 13–18 April 2008, European Geophysical Union, 2008.
- Lisiecki, L. E. and Raymo, M. E.: A Pliocene-Pleistocene stack of 57 globally distributed benthic $\delta^{18}\text{O}$ records, *Paleoceanography*, 20, PA1003, doi:10.1029/2004PA001071, 2005.
- Loulergue, L., Schilt, A., Spahni, R., Masson-Delmotte, V., Blunier, T., Lemieux, B., Barnola, J.-M., Raynaud, D., Stocker, T. F., and Chappellaz, J.: Orbital and millennial-scale features of atmospheric CH_4 over the past 800 000 years, *Nature*, 453, 383–386, doi:10.1038/nature06950, 2008.
- Lüthi, D., Le Floch, M., Bereiter, B., Blunier, T., Barnola, J.-M., Siegenthaler, U., Raynaud, D., Jouzel, J., Fischer, H., Kawamura, K., and Stocker, T. F.: High-resolution carbon dioxide concentration record 650 000–800 000 years before present, *Nature*, 453, 379–382, doi:10.1038/nature06949, 2008.

- Montagnat, M., Duval, P., Bastie, P., Hamelin, B., de Angelis, M., Petit, J. R., and Lipenkov, V. Y.: High crystalline quality of large single crystals of subglacial ice above Lake Vostok (Antarctica) revealed by hard X-ray diffraction, *C.R. Acad. Sc. Paris, Série IIa Sciences de la Terre et des Planètes*, 333, 419–425, 2001.
- Mulvaney, R., Wolff, E.W., and Oates, K.: Sulphuric acid at grain boundaries in Antarctic ice, *Nature*, 331, 247–249, 1988.
- Ohno, H., Igarashi, M., and Hondoh, T.: Salt inclusions in polar ice cores: Location and chemical form of water-soluble impurities, *Earth Planet. Sci. Lett.*, 232, 171–178, 2005.
- Parrenin, F., Barnola, J. M., Beer, J., Blunier, T., Castellano, E., Chappellaz, J. A., Dreyfus, G., Fisher, H., Fujita, S., Jouzel, J., Kawamura, K., Lemieux-Dudon, B., Masson-Delmotte, V., Narasi, B.M., Petit, J.-R., Raisbeck, J., Raynaud, D., Ruth, U., Schwander, J., Severi, M., Spahni, R., Steffensen, J. P., Svensson, A. M., Udisti, R., Waelbroek, C., and Wolff, E. W.: The EDC chronology for the EPICA Dome C ice core, *Clim. Past*, 3, 485–497, doi:10.5194/cp-3-485-2007, 2007.
- Petit, J., Jouzel, J., Raynaud, D., Barkov, N., Barnola, J.M., Basile, I., Bender, M., Chappellaz, J., Davis, M., Delaygue, G., Delmotte, M., Kotlyakov, V., Legrand, M., Lipenkov, V., Lorius, C., Pépin, L., Ritz, C., Saltzman, E., and Stievenard, M.: Climate and atmospheric history of the past 420 000 years from the Vostok ice core, Antarctica, *Nature*, 399, 429–436, 1999.
- Pol, K., Masson-Delmotte, V., Johnsen, S., Bigler, M., Cattani, O., Durand, G., Falourd, S., Jouzel, J., Minster, B., Parrenin, F., Ritz, C., Steen-Larsen, H. C., and Stenni, B.: New MIS 19 EPICA Dome C high resolution deuterium data: Hints for a problematic preservation of climate variability at sub-millennial scale in the “oldest ice”, *Earth Planet. Sci. Lett.*, 298, 1/2, 95–103, 2010.
- Pol, K., Debret, M., Masson-Delmotte, V., Capron, E., Cattani, O., Dreyfus, G., Falourd, S., Johnsen, S., Jouzel, J., Landais, A., Minster, B., and Stenni, B.: Links between MIS 11 millennial to sub-millennial climate variability and long term trends as revealed by new high resolution EPICA Dome C deuterium data – A comparison with the Holocene, *Clim. Past*, 7, 437–450, doi:10.5194/cp-7-437-2011, 2011.
- Raisbeck, G. M., Yiou, F., Cattani, O., and Jouzel, J.: ^{10}Be evidence for the Matuyama-Brunhes geomagnetic reversal in the EPICA Dome C ice core, *Nature*, 444, 82–84, doi:10.1038/nature05266, 2006.
- Raynaud D., Barnola, J.-M., R. Souchez, R. Lorrain, Petit J.-R., Duval P., and Lipenkov V.: The record for marine isotopic stage 11, *Nature*, 436, 30–40, 2005.
- Raynaud, D., Lipenkov, V., Lemieux-Dudon, B., Duval, P., Loutre, M.-F., and Lhomme, N.: The local insulation signature of air content in Antarctic ice. A new step toward an absolute dating of ice records, *Earth Planet. Sci. Lett.*, 261, 337–349, 2007.
- Rempel, A.: Englacial phase changes and intergranular flow above subglacial lakes, *Ann. Glaciol.*, 40, 191–194, 2005.
- Rempel, A. W., Waddington, E. D., Wettlaufer, J. S., and Worster, M. G.: Possible displacement of the climate signal in ancient ice by premelting and anomalous diffusion, *Nature*, 411, 568–571, 2001.
- Rempel, A. W., Wettlaufer, J. S., and Waddington, E. D.: Anomalous diffusion of multiple impurity species: predicted implications for the ice core climate record, *J. Geophys. Res.*, 107, 2330, doi:10.1029/2002JB001857, 2002.
- Rempel, A. W.: Segregation, transport and interaction of climate proxies in polycrystalline ice, *Can. J. Phys.*, 81, 89–97, 2003.
- Remy, F. and Tabacco, I. E.: Bedrock features and ice flow near the EPICA ice core site (Dome C, Antarctica), *Geophys. Res. Lett.*, 27, 405–408, 2000.
- Schilt, A., Baumgartner M., Blunier T., Schwander J., Spahni R., Fischer H., and Stocker, T. F.: Glacial-interglacial and millennial-scale variations in the atmospheric nitrous oxide concentration during the last 800 000 years, *Quat. Sci. Rev.*, 29, 182–192, doi:10.1016/j.quascirev.2009.03.011, 2010.
- Souchez, R.: The build up of the ice sheet in Central Greenland, *J. Geophys. Res.*, 102, 26317–26323, 1997.
- Souchez, R. and Lorrain, R.: Ice composition and glacier dynamics, Heidelberg, Springer-Verlag, 0 387 52521 1, 207 pp., 1991.
- Souchez, R., Lorrain, R., Tison, J.-L., and Jouzel, J.: Co-isotopic signature of two mechanisms of basal-ice formation in Arctic outlet glaciers, *Ann. Glaciol.*, 10, 163–166, 1988.
- Souchez, R., Lemmens, M., Tison, J.-L., Lorrain, R., and Janssens, L.: Reconstruction of basal boundary conditions at the Greenland Ice Sheet margin from gas composition in the ice, *Earth Planet. Sci. Lett.*, 118, 327–333, 1993.
- Souchez, R., Tison, J. L., Lorrain, R., Janssens, L., Stievenard, M., Jouzel, J., Sveinbjörnsdottir, A., and Johnsen, S. J.: Stable isotopes in the basal silty ice preserved in the Greenland Ice Sheet at Summit; Environmental implications, *Geophys. Res. Lett.*, 21, 693–696, 1994.
- Souchez, R., Janssens, L., Lemmens, M., and Stauffer, B.: Very low oxygen concentration in basal ice from Summit, Central Greenland, *Geophys. Res. Lett.*, 22, 2001–2004, 1995a.
- Souchez, R., Lemmens, M., and Chappellaz, J.: Flow-induced mixing in the GRIP basal ice deduced from the CO_2 and CH_4 records, *Geophys. Res. Lett.*, 22, 41–44, 1995b.
- Souchez, R., Bouzette, A., Clausen, H., Johnsen, S., and Jouzel, J.: A stacked mixing sequence at the base of the Dye 3 core, Greenland, *Geophys. Res. Lett.*, 25, 1943–1946, 1998.
- Souchez, R., Petit, J. R., Tison, J. L., Jouzel, J., and Verbeke, V.: Ice formation in subglacial Lake Vostok, Central Antarctica, *Earth Planet. Sci. Lett.*, 181, 529–538, 2000a.
- Souchez, R., Vandenschrick, G., Lorrain, R., and Tison, J.-L.: Basal ice formation and deformation in Central Greenland : a review of existing and new ice core data, in: *Deformation of Glacial Materials*, edited by: Maltman, A. J., Hubbard, B., and Hambrey, M., Special Publication no. 176, 13–22, 2000b.
- Souchez, R., Jean-Baptiste, R., Petit, J. R., Lipenkov, V., and Jouzel, J.: What is the deepest part of the Vostok ice core telling us?, *Earth Sci. Rev.*, 60, 131–146, 2002a.
- Souchez, R., Petit, J. R., Jouzel, J., Simões, J., de Angelis, M., Barkov, N., Stievenard, M., Vimeux, F., Sleewaegen, S., and Lorrain, R.: Highly deformed basal ice in the Vostok core, Antarctica, *Geophys. Res. Lett.*, 29, 4041–4044, 2002b.
- Souchez, R., Petit, J.-R., Jouzel, J., de Angelis, M., and Tison, J. L.: Reassessing Lake Vostok’s behaviour from existing and new ice core data, *Earth Planet. Sci. Lett.*, 217, 163–170, 2003.
- Souchez, R., Jouzel, J., Landais, A., Chappellaz, J., Lorrain, R., and Tison, J.-L.: Gas isotopes in ice reveal a vegetated central Greenland during ice sheet invasion, *Geophys. Res. Lett.*, 33, L24503, doi:10.1029/2006GL028424, 2006.
- Stenni, B., Masson-Delmotte, V., Selmo, E., Oerter, H., Meyer, H., Rothlisberger, R., Jouzel, J., Cattani, O., Falourd, S., Fisher, H.,

- Hoffmann, G., Iacumin, P., Johnsen, S., Minster, B., and Udisti, R.: The deuterium excess records of EPICA Dome C and Dronning Maud Land ice cores (East Antarctica), *Quat. Sci. Rev.*, 29, 146–159, 2010.
- Tabacco, I.E., Passerini, A., Corbelli, F., and Gorman, M.: Determination of the surface and bed topography at Dome C, East Antarctica, *J. Glaciol.*, 44, 185–191, 1998.
- Tison, J.-L. and Lorrain, R.: A mechanism of basal ice layer formation involving major ice-fabrics changes, *J. Glaciol.*, 33, 47–50, 1987.
- Tison, J.-L., Souchez, R., and Lorrain, R.: On the incorporation of unconsolidated sediments in basal ice: present-day examples, *Zeit. Geomorphology*, 72, 173–183, 1989.
- Tison, J.-L., Petit, J. R., Barnola, J. M., and Mahaney, W. C.: Debris entrainment at the ice-bedrock interface in sub-freezing temperature conditions (Adélie Land, Antarctica), *J. Glaciol.*, 39, 303–315, 1993.
- Tison, J.-L., Thorsteinsson, T., Lorrain, R., and Kipfstuhl, J.: Origin and development of textures and fabrics in basal ice at Summit, Central Greenland, *Earth Planet. Sci. Lett.*, 125, 421–437, 1994.
- Tison, J.-L., Souchez, R., Wolff, E. W., Moore, J. C., Legrand, M. R., and de Angelis, M.: Is a periglacial biota responsible for enhanced dielectric response in basal ice from the Greenland Ice Core Project ice core?, *J. Geophys. Res.*, 103, 18885–18894, 1998.
- Traversi, R., Becagli, S., Castellano, E., Marino, F., Severi, M., Udisti, R., Kaufmann, P., Lambert, F., Stauffer, B., Hansson, M., Petit, J. R., Ruth, U., Raisbeck, G., and Wolff, E. W.: Chemical characterization of peculiar ice layers at the bottom of the EPICA-DC ice core, *Geophysical Research Abstracts*, 8, 07199, European Geosciences Union General Assembly 2006, 02-07 April 2006, EGU, 2006.
- Traversi, R., Becagli, S., Castellano, E., Marino, F., Rugi, F., Severi, M., de Angelis, M., Fisher, H., Hansson, M., Steffensen, J. P., Wolff, E. W., and Udisti, R.: Sulfate spikes at the bottom of the EDC core: evidence of glaciological artefacts, *Environ. Sci. Technol.*, 43, 8737–8743, 2009.
- Urbini, S., Frezzotti, M., Gandolfi, S., Vincent, C., Scarchilli, C., Vittuari, L., and Fily, M.: Historical behaviour of Dome C and Talos Dome (East Antarctica) as investigated by snow accumulation and ice velocity measurements, *Glob. Planet. Change*, 60, 576–588, 2008.
- Verbeke, V., Lorrain, R., Johnsen, S. J., and Tison, J.-L.: A multiple-step deformation history of basal ice from the Dye3 (Greenland) core: new insights from the CO₂ and CH₄ content, *Ann. Glaciol.*, 35, 231–236, 2002.
- Weis, D., Demaiffe, D., Souchez, R., Gow, A. J., and Meese, D. A.: Nd, Sr and Pb isotopic compositions of basal material in Central Greenland: inferences for ice sheet development, *Earth Planet. Sci. Lett.*, 150, 161–169, 1997.
- Wettlaufer, J. S.: Impurity effects in the Premelting of ice, *Phys. Rev. Lett.*, 82, 2516–2519, 1999.
- Wolff, E. W., Fisher, H., Fundel, F., Ruth, U., Twarloh, B., Littot, G. C., Mulvaney, R., Röthlisberger, R., de Angelis, M., Boutron, C. F., Hansson, M., Jonsell, U., Hutterli, M. A., Lambert, F., Kaufmann, P., Stauffer, B., Stocker, T. F., Steffensen, J. P., Bigler, M., Siggaard-Andersen, M. L., Udisti, R., Becagli, S., Castellano, E., Severi, M., Wagenbach, D., Barbante, C., Gabrielli, P., and Gaspari, V.: Southern Ocean sea-ice extent, productivity and iron flux over the past eight glacial cycles, *Nature*, 440, 491–496, doi:10.1038/nature04614, 2006.